Softening of Roton and Phonon Modes in a Bose-Einstein Condensate with Spin-Orbit Coupling

Si-Cong Ji, Long Zhang, Xiao-Tian Xu, Zhan Wu, Youjin Deng, Shuai Chen,* and Jian-Wei Pan†

Shanghai Branch, Hefei National Laboratory for Physical Sciences at Microscale and Department of Modern Physics, University of Science and Technology of China, Shanghai 201315, China

and Synergetic Innovation Center of Quantum Information and Quantum Physics, University of Science and Technology of China, Hefei, Anhui 230026, China

(Received 7 August 2014; revised manuscript received 29 December 2014; published 9 March 2015)

Roton-type excitations usually emerge from strong correlations or long-range interactions, as in superfluid helium or dipolar ultracold atoms. However, in a weakly short-range interacting quantum gas, the recently synthesized spin-orbit (SO) coupling can lead to various unconventional phases of superfluidity and give rise to an excitation spectrum of roton-maxon character. Using Bragg spectroscopy, we study a SO-coupled Bose-Einstein condensate of ^{87}Rb atoms and show that the excitation spectrum in a "magnetized" phase clearly possesses a two-branch and roton-maxon structure. As Raman coupling strength Ω is decreased, a roton-mode softening is observed, as a precursor of the phase transition to a stripe phase that spontaneously breaks spatially translational symmetry. The measured roton gaps agree well with theoretical calculations. Furthermore, we determine sound velocities both in the magnetized and in the nonmagnetized phases, and a phonon-mode softening is observed around the phase transition in between. The validity of the f-sum rule is examined.

DOI: 10.1103/PhysRevLett.114.105301 PACS numbers: 67.85.De, 03.75.Kk, 67.85.Fg

The roton and phonon are two typical excitation modes of superfluids. They were first introduced by Landau in his phenomenological explanation on the superfluidity of liquid helium [1,2], and an experimental observation was realized about two decades later [3,4]. The emergence of the roton mode in superfluid helium originates from strong density correlations. In weakly interacting ultracold quantum gases, the roton-maxon dispersion structures were predicted in the systems with long-range interactions [5–8], which were recently observed in the system of a Bose-Einstein condensate (BEC) interacting with a cavity [9]. Across the phase transition from a superfluid to a supersolid phase, a softening of the roton mode was further demonstrated [9]. An important question naturally arises: can an excitation spectrum of roton-maxon character be observed in a quantum gas with weak and short-range interactions?

Recently, artificial one-dimensional spin-orbit (SO) coupling has been synthesized in ultracold bosonic [10,11] and fermionic [12,13] atoms by two counterpropagating Raman lasers that couple the momentum of an atom to its spin [14]. The single-particle dispersion is significantly modified such that a degenerate double-well structure appears for some Raman-coupling strength Ω. Despite the fact that interatomic interactions are weak and short ranged, these systems can exhibit many unconventional condensate phases. For ^{87}Rb atoms, as Ω increases, the ground-state phase diagram is predicted to include [15,16] a stripe phase of periodic density fringes that breaks translational symmetry, a "magnetized" phase breaking a discrete Z_2 symmetry, and a nonmagnetic phase. This rich structure of phase diagram has been largely supported by experiments [10], and its finite-temperature analog has also been explored [17].

This recent very significant experimental progress in manipulating SO coupling paves the way to addressing the aforementioned question. It is recognized that superfluids with a tendency towards periodic order can have phonon- and roton-type excitation modes. In a SO-coupled condensate of ^{87}Rb atoms, the occurrence of the stripe phase preceding the magnetized phase indicates that the excitation spectrum in the latter exhibits a roton-maxon structure [18–20]. As the phase boundary is approached, a roton-mode softening is further expected. In this work, we experimentally demonstrate such a structure and, thus, provide the first direct experimental observation of the roton mode and its softening in weak and short-range interacting systems.

The experimental setup is sketched in Fig. 1(a), showing much similarity to our previous work [11,17]. A BEC of about 1.5×10^5 ^{87}Rb atoms is prepared in a crossed dipole trap with frequency $\omega = 2\pi \times \{45, 45, 55\}$ Hz. A bias magnetic field along the z axis is applied to generate the Zeeman splitting. The two counterpropagating Raman lasers with wavelength $\lambda_\Omega = 803.2$ nm and relative angle $\theta_\Omega = 105°$ are applied to couple the three internal states of the $F = 1$ manifold to generate the SO coupling. In addition, the SO-coupled BEC is illuminated by two Bragg beams with parallel polarization, which are symmetric about the y axis.

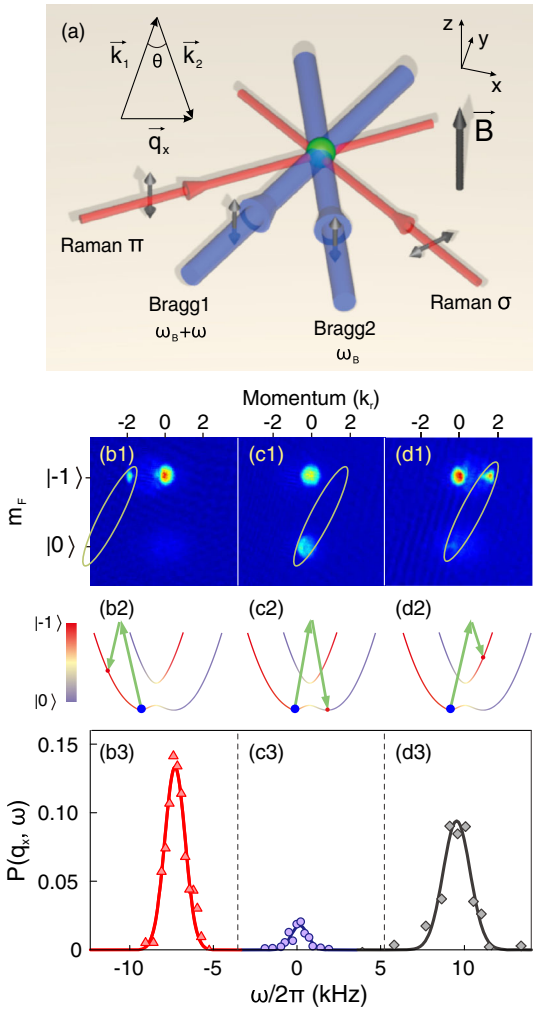

FIG. 1 (color online). Experimental setup and Bragg spectroscopy. (a) In the x-y plane, there are a pair of Raman lasers with relative angle 105° and two Bragg beams separated by an angle $3° \leq \theta \leq 180°$, which can produce a momentum transfer in the x direction with $0.07k_r \leq |q_x| \leq 2.60k_r$. A bias magnetic field in the z direction generates the Zeeman splitting. [(b)–(d)] Spin-resolved TOF images (b1)–(d1), schematic diagrams of excitations (b2)–(d2), and excitation efficiency $P(q_x, \omega)$ in (b3)–(d3) for $\Omega = 2E_r$, with $\theta = 86°$, $|q_x| = 1.77k_r$. The ellipses mark atoms kicked out by the Bragg pulse. The excitation frequencies ω are, respectively, −7.38 kHz (b1), 0.23 kHz (c1), and 9.60 kHz (d1). The color bar in the second row indicates the spin proportion of each dressed state. The curves in (b3)–(d3) correspond to the Gaussian fits.

By a relatively large quadratic Zeeman shift, the $|m_F = 1\rangle$ state can be effectively eliminated, and the system can be regarded as a spin-1/2 system. The single-particle Hamiltonian along the SO coupling direction (the x direction) is given by ($\hbar = 1$)

$$H_0 = \frac{(k_x - k_r\sigma_z)^2}{2m} + \frac{\delta}{2}\sigma_z + \frac{\Omega}{2}\sigma_x, \qquad (1)$$

where $k_r = (2\pi/\lambda_\Omega)\sin(\theta_\Omega/2)$ is the recoil momentum of Raman coupling, m is the atom mass, Ω is the Raman coupling strength, δ is the two-photon detuning, which is fine tuned to be $\delta = 0$ in the experiment, and σ_z and σ_x represent the Pauli matrices, with $|m_F = -1\rangle$ for spin $|\uparrow\rangle$ and $|m_F = 0\rangle$ for spin $|\downarrow\rangle$. For each given k_x, Eq. (1) has two eigenstates with energy $\mathcal{E}_+(k_x) > \mathcal{E}_-(k_x)$ for the upper (+) and the lower (−) branch of single-particle dispersion [20,21], respectively. The lower branch has two degenerate minima for $\Omega < 4E_r$ ($E_r = k_r^2/2m$), denoted by $\pm k_{\min}$ [$k_{\min} = k_r\sqrt{1 - (\Omega/4E_r)^2}$], and has a single minima at $k_x = 0$ for $\Omega > 4E_r$. With interatomic interactions of ^{87}Rb atoms being taken into account, it has been shown [10,16] that atoms condense in a superposition state $(|+k_{\min}\rangle + |-k_{\min}\rangle)/\sqrt{2}$ for $\Omega < 0.2E_r$, exhibiting the stripe order. For $0.2E_r < \Omega < 4E_r$, the system maintains the magnetized phase, where atoms condenses at $k_{\min}$ or $-k_{\min}$. When $\Omega > 4E_r$, the single-particle dispersion has only one single minimum at zero momentum, and the Bose gas, hence, exhibits no magnetization, i.e., the nonmagnetized phase.

The excitation spectrum of the magnetized phase is measured through Bragg spectroscopy [22–27]. The BEC is prepared at the spin state $|m_F = -1\rangle$. The Raman coupling strength Ω is adiabatically ramped up to the desired value, and the condensate is loaded to the dressed state $-k_{\min}$; see the Supplemental Material [28]. Then, we quickly switch on two Bragg lasers for 1–2 ms. The Bragg beams are set with wavelength $\lambda_B = 780.24$ nm and 6.8 GHz detuned away from the resonance. The angle θ between the two lasers [Fig. 1(a)] determines the momentum transfer $q_x = 2k_B\sin(\theta/2)$ ($k_B = 2\pi/\lambda_B$), while the frequency difference ω is tuned to produce an excitation. The Bragg pulse kicks a small percent of atoms out of the condensate cloud. The intensity of the Bragg lasers is adjusted to excite at most 20% atoms, such that the linear response theory applies [29]. Finally, with the Stern-Gerlach technique, we take spin-resolved time-of-fight (TOF) images after 24 ms of free expansion. Three typical examples for $\Omega = 2E_r$ are shown in Figs. 1(b)–1(d). The angle between the two Bragg beams is set to $\theta \approx 86°$, with the momentum transfers $|q_x| = 1.77k_r$, close to the separation $\sqrt{3}k_r$ of the two minima of the single-particle dispersion. Note that Figs. 1(c) and 1(d), with the same q_x value but different ω values, correspond to excitations to different energy branches. Furthermore, the spins of atoms in Fig. 1(c) flip when being kicked out from the condensate by the Bragg pulse. This is due to the lock of spin and momentum [21].

For each TOF image, the atom numbers in the Bragg cloud and the remaining condensate, N_B and N_c, are counted, and the ratio $P(q_x, \omega) \equiv N_B/(N_B + N_c)$ is calculated. For a given momentum transfer q_x, a broad range of frequency difference ω is scanned with the Rabi frequency Ω_B of the Bragg beams being fixed at an appropriate value. For $\Omega = 2E_r$, Figs. 1(b3)–1(d3) show the plot of the

excitation efficiency $P(q_x, \omega)$ versus frequency difference ω, for $q_x = -1.77k_r$ (red triangles) and $1.77k_r$ (purple circles and gray diamonds). It can be seen that there are two resonance peaks for momentum transfer $q_x = 1.77k_r$, corresponding to the lower and upper branches of the excitation spectra, respectively. The measured data are fitted by a Gaussian curve, and the peak frequency is used to identify the excitation energy (see the Supplemental Material [28]). All the whole excitation spectra for a fixed Raman coupling Ω are then constructed by varying momentum transfer q_x; see Fig. 2(a) for $\Omega = 2E_r$.

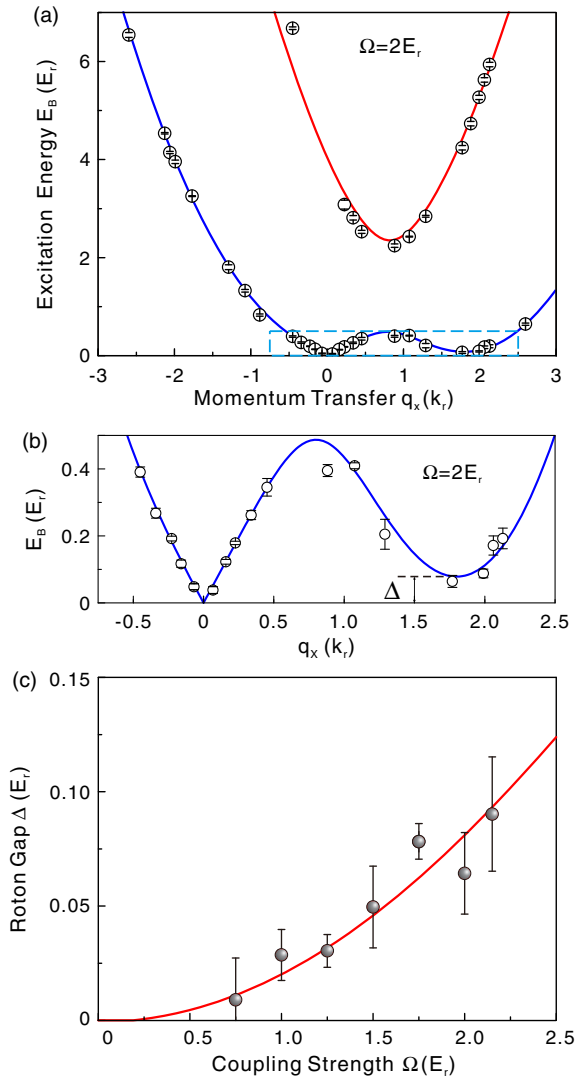

FIG. 2 (color online). Excitation spectrum and roton mode softening. (a) Excitation spectrum for $\Omega = 2E_r$. The two branches of spectra are clearly seen and agree well with theoretical calculations (blue and red solid curves) based on a modified Bogoliubov theory. (b) Zoom in of the low-energy part (dashed box) of the excitation spectrum in (a), which clearly shows a roton-maxon structure. (c) Softening of roton mode. The measured roton gap Δ (circles) becomes smaller as Ω decreases and vanishes for small Ω.

The lower branch of the excitation spectrum in the magnetized phase clearly shows a roton-type minimum at finite momentum around $q_x = 2k_{\min}$ [see Fig. 2(b)]. We measure the roton gap Δ, defined as the excitation energy at the roton minimum, and find it softens as Raman coupling strength decreases [Fig. 2(c)]. We calculate the roton gap based on a modified Bogoliubov theory [19,20], and the results are shown as the red solid curve in Fig. 2(c). The experimental data agree well with theoretical calculations. As mentioned above, for ^{87}Rb atoms, there is a phase transition near $\Omega_1 \approx 0.2E_r$ between the magnetized and the stripe phase, and accordingly, the roton gap is expected to vanish at Ω_1. Unfortunately, our experimental data are not sufficiently accurate to figure out the precise location of Ω_1. On the other hand, we do find that the roton-maxon structure disappears when Ω is tuned above a large enough value (about $3.4E_r$ in our experiment), suggesting that the roton mode is a precursor of the stripe phase with periodic fringes.

The observed softening of the roton gap can find its origin in a Raman-dressed interaction. In the presence of SO coupling, interatomic interaction becomes anisotropic [30], and this anisotropy can be tuned by varying Ω [31]. This can be revealed by calculating the interaction energy for a condensate of different components. As shown in Ref. [10], for ^{87}Rb atoms, we have interaction energy $E_I \approx 1/2 \int d^3\mathbf{r}\{(c_0 + c_2/2)[n_{\uparrow'}(\mathbf{r}) + n_{\downarrow'}(\mathbf{r})]^2 + c_2/2[n_{\uparrow'}(\mathbf{r})^2 - n_{\downarrow'}(\mathbf{r})^2] + (c_2 + c_0\Omega^2/8E_r^2)n_{\uparrow'}(\mathbf{r})n_{\downarrow'}(\mathbf{r})\}$, where the spin-independent interaction $c_0 = 7.79 \times 10^{-12}$ Hz cm^3, the spin-dependent interaction $c_2 = -3.61 \times 10^{-14}$ Hz cm^3, and $n_{\uparrow'}(\mathbf{r})$ and $n_{\downarrow'}(\mathbf{r})$ respectively represent the spatial density of the components at $-k_{\min}$ and $k_{\min}$. This means that the interaction energy for a condensate of two dressed components $\pm k_{\min}$ has additional energy terms compared to the energy for a single-component condensate at $k_{\min}$ or $-k_{\min}$. Accordingly, one can give an estimation of the roton gap as $\Delta \approx c_0 n(\Omega - \Omega_1)^2/16E_r^2$ for $\Omega > \Omega_1$ with n for the condensate density and $\Omega_1 \approx 0.2E_r$.

We also measure sound velocities both in the magnetized and in the nonmagnetized phase and find a softening of the phonon mode near the phase transition between these two phases. In the magnetized phase, the excitation spectrum exhibits linear dispersions in the long wavelength limit, i.e., $E_B(q_x) = -c_1 q_x$ for $q_x < 0$ and $E_B(q_x) = c_2 q_x$ for $q_x > 0$; see Fig. 2(b). Here, c_1 (c_2) is the sound velocity in the negative (positive) x direction. The measured velocities c_1 and c_2 are almost identical for a given Ω (Fig. 3), since the interaction difference in ^{87}Rb atoms is very small [19]. The values of c_1 and c_2 decrease as Ω is enhanced and reach a minimum near the phase transition Ω_2 that is slightly above $4E_r$, as shown in Fig. 3. For $\Omega > \Omega_2$, heating from Raman lasers makes it difficult to adiabatically load BEC into the minimum, and the condensate starts to oscillate in the trap during the Bragg pulse. To minimize effect of the induced Doppler shift, the sound velocity in the nonmagnetized

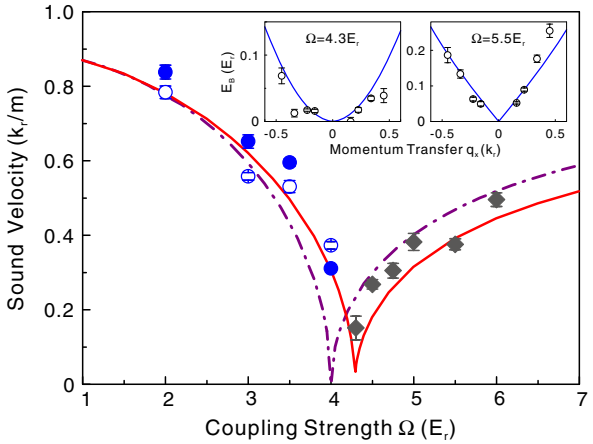

FIG. 3 (color online). Softening of phonon mode. Sound velocities c_1 (solid circles) and c_2 (open circles) are both plotted for $\Omega < 4.3E_r$. For $\Omega \geq 4.3E_r$, the sound velocity (diamonds) is taken as the average of the measurements in the negative and positive x directions to minimize possible Doppler effect. Theoretical calculations for a spin-1/2 system (dot-dashed curve) predict a vanishing minimum at the phase transition point $\Omega = 4E_r$. A more practical consideration based on a spin-1 system with the effectively suppressed state $|m_F = 1\rangle$ (solid curve) shows that the sound velocity cannot touch zero, and the minimum is shifted to about $4.3E_r$ for the set quadratic Zeeman shift $\epsilon = 4.53E_r$. The insets show the low-energy excitation spectrum for $\Omega = 4.3E_r$ (left), where the spectrum becomes parabolalike, and $\Omega = 5.5E_r$ (right), where the linear mode recovers.

phase is taken as the average of the values for $q_x < 0$ and $q_x > 0$. Nevertheless, it is still clear that the sound velocity increases with the coupling strength.

The nonmonotonic behavior of the sound velocity as shown in Fig. 3 can be interpreted by the modification of single-particle dispersion. With the effective-mass approximation, the sound velocity c_s ($c_1 = c_2 = c_s$ is assumed) can be written as $c_s = \sqrt{gn/m^*}$ [20]. Here, the effective mass m^* is given by $m^* = m(1 - \Omega^2/16E_r^2)^{-1}$ for $\Omega < 4E_r$ and $m^* = m(1 - 4E_r/\Omega)^{-1}$ for $\Omega > 4E_r$. This shows that the vanishing of sound velocity originates in the divergency of the effective mass at $\Omega = 4E_r$, which marks the transition point between the magnetized and the nonmagnetized phase. However, the Bose gas in our experiment is not a pure spin-1/2 system. Because of the influence of the suppressed state $|m_F = 1\rangle$, the value of sound velocity cannot drop to zero and the transition point is shifted to about $\Omega = 4.3E_r$ (Fig. 3).

Phonon mode softening indicates that at the transition point, the Bose gas should exhibit no superfluidity when an impurity moves inside with finite velocity in the SO coupling direction. It should be pointed out that due to the absence of Galilean invariance [11] in a SO-coupled system, a moving SO-coupled Bose gas has a different excitation spectrum from what we measure in Fig. 2, and softening of the phonon mode is prevented in the comoving frame [20].

To illustrate the validity of the Bragg spectroscopy in SO-coupled systems, we examine the sum rules [29], which concern the moments of the dynamic structure factor, defined as $M_p(q_x) \equiv \int \omega^p S(q_x, \omega) d\omega$, where $p \geq 0$ is an integer. The zeroth-order moment for $p = 0$ relates to the static structure factor as $M_0(q_x) = NS(q_x)$ with N the number of atoms, which reflects the excitation probability by Bragg scattering with momentum transfer q_x. In Fig. 4(a), we plot $S(q_x)$ for $\Omega = 2E_r$ as a function of q_x (the red circles), where $S(q_x)$ is normalized so that its maximum is equal to unity. The blue circles in Fig. 4(a) represent the contribution $S_-(q_x)$ from the lower branch of the excitation spectrum. The theoretical calculations based on local density approximation (shown as the solid lines) agree with experimental data, except for those three points with very small momentum transfer q_x. The relative contribution $S_-(q_x)/S(q_x)$ is shown in the inset of Fig. 4(a), which rapidly decreases as the momentum transfer becomes larger. The famous f-sum rule is about the energy-weighted moment $M_1(q_x)$ and states that $M_1(q_x) = Nq_x^2/2m$, where m is the mass of the atom. The validity of the f-sum rule in a SO-coupled system has been theoretically examined in Ref. [19]. The measured first moment $M_1(q_x)$ for $\Omega = 2E_r$ is plotted versus q_x in Fig. 4(b). These experimental data can be well described by a quadratic curve, demonstrating the validity of the f-sum rule at least in the magnetized phase.

We have shown that despite interatomic interactions that are weak and short-ranged, the SO-coupled ^{87}Rb condensate has an excitation spectrum of roton-maxon character in the magnetized phase, which softens near the phase transition to the stripe phase. The sound velocities are also measured, and a phonon-mode softening is observed. We mention that in condensed-matter physics and ultracold

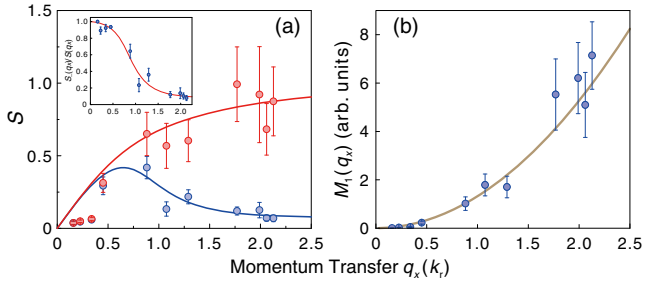

FIG. 4 (color online). Sum rules for $\Omega = 2E_r$. (a) Static structure factor $S(q_x)$ (red circles) and the contribution $S_-(q_x)$ (blue circles) from the lower branch of the excitation spectrum. The theoretical calculations based on local density approximations are shown as red and blue solid curves. The relative contribution $S_-(q_x)/S(q_x)$ is shown in the inset. (b) Energy-weighted moment $M_1(q_x)$. The good agreement between the experimental data (blue circles) demonstrates the validity of the f-sum rule.

atomic physics, the measurement of excitation spectrum is in itself of an important role in revealing the properties of low-temperature phases [32]. The observed linear dispersion near $q_x = 0$ is an important feature of superfluidity. Furthermore, the measured roton-maxon structure of excitation spectrum, its disappearance for large Ω, and the softening of the roton gap strongly support the predicted ground-state phase diagram for the SO-coupled Bose gas of ^{87}Rb atoms.

This work has been supported by the NNSF of China, the CAS, and the National Fundamental Research Program (under Grants No. 2011CB921300 and No. 2013CB922001).

We acknowledge insightful discussions with H. Zhai, C. Chin, S. Stringari, Y. Li, and Z. Q. Yu. S.-C. J. and L. Z. contributed equally to this work.

*shuai@ustc.edu.cn
†pan@ustc.edu.cn

[1] L. D. Landau, J. Phys. USSR **5**, 71 (1941).
[2] L. D. Landau, J. Phys. USSR **11**, 91 (1947).
[3] J. L. Yarnell, G. P. Arnold, P. J. Bendt, and E. C. Kerr, Phys. Rev. Lett. **1**, 9 (1958).
[4] D. G. Henshaw and A. D. B. Woods, Phys. Rev. **121**, 1266 (1961).
[5] D. H. J. O'Dell, S. Giovanazzi, and G. Kurizki, Phys. Rev. Lett. **90**, 110402 (2003).
[6] L. Santos, G. V. Shlyapnikov, and M. Lewenstein, Phys. Rev. Lett. **90**, 250403 (2003).
[7] F. S. Nogueira and H. Kleinert, Phys. Rev. B **73**, 104515 (2006).
[8] N. Henkel, R. Nath, and T. Pohl, Phys. Rev. Lett. **104**, 195302 (2010).
[9] R. Mottl, F. Brennecke, K. Baumann, R. Landig, T. Donner, and T. Esslnger, Science **336**, 1570 (2012).
[10] Y.-J. Lin, K. Jiménez-García, and I. B. Spielman, Nature (London) **471**, 83 (2011).
[11] J.-Y. Zhang *et al.*, Phys. Rev. Lett. **109**, 115301 (2012).
[12] P. Wang, Z.-Q. Yu, Z. Fu, J. Miao, L. Huang, S. Chai, H. Zhai, and J. Zhang, Phys. Rev. Lett. **109**, 095301 (2012).
[13] L. W. Cheuk, A. T. Sommer, Z. Hadzibabic, T. Yefsah, W. S. Bakr, and M. W. Zwierlein, Phys. Rev. Lett. **109**, 095302 (2012).
[14] V. Galitski and I. B. Spielman, Nature (London) **494**, 49 (2013).
[15] T.-L. Ho and S. Zhang, Phys. Rev. Lett. **107**, 150403 (2011).
[16] Y. Li, L. P. Pitaevskii, and S. Stringari, Phys. Rev. Lett. **108**, 225301 (2012).
[17] S.-C. Ji, J.-Y. Zhang, L. Zhang, Z.-D. Du, W. Zheng, Y.-J. Deng, H. Zhai, S. Chen, and J.-W. Pan, Nat. Phys. **10**, 314 (2014).
[18] W. Zheng and Z. Li, Phys. Rev. A **85**, 053607 (2012).
[19] G. I. Martone, Y. Li, L. P. Pitaevskii, and S. Stringari, Phys. Rev. A **86**, 063621 (2012).
[20] W. Zheng, Z.-Q. Yu, X. Cui, and H. Zhai, J. Phys. B **46**, 134007 (2013).
[21] H. Zhai, Rep. Prog. Phys. **78**, 026001 (2015).
[22] J. Stenger, S. Inouye, A. Chikkatur, D. Stamper-Kurn, D. Pritchard, and W. Ketterle, Phys. Rev. Lett. **82**, 4569 (1999).
[23] D. Stamper-Kurn, A. Chikkatur, A. Görlitz, S. Inouye, S. Gupta, D. Pritchard, and W. Ketterle, Phys. Rev. Lett. **83**, 2876 (1999).
[24] J. Steinhauer, R. Ozeri, N. Katz, and N. Davidson, Phys. Rev. Lett. **88**, 120407 (2002).
[25] G. Veeravalli, E. Kuhnle, P. Dyke, and C. J. Vale, Phys. Rev. Lett. **101**, 250403 (2008).
[26] S. B. Papp, J. M. Pino, R. J. Wild, S. Ronen, C. E. Wieman, D. S. Jin, and E. A. Cornell, Phys. Rev. Lett. **101**, 135301 (2008).
[27] P. T. Ernst, S. Götze, J. S. Krauser, K. Pyka, D.-S. Lühmann, D. Pfannkuche, and K. Sengstock, Nat. Phys. **6**, 56 (2010).
[28] See Supplemental Material at http://link.aps.org/supplemental/10.1103/PhysRevLett.114.105301 for data analysis.
[29] L. P. Pitaevskii and S. Stringari, *Bose-Einstein Condensation* (Oxford University Press, New York, 2003).
[30] L. Zhang, Y. Deng, and P. Zhang, Phys. Rev. A **87**, 053626 (2013).
[31] R. A. Williams, L. J. LeBlanc, K. Jimenez-Garcia, M. C. Beeler, A. R. Perry, W. D. Phillips, and I. B. Spielman, Science **335**, 314 (2012).
[32] A. Griffin, *Excitations in a Bose-Condensed Liquid* (Cambridge University Press, New York, 1993).